Two-Dimensional Aeroelastic Limit Cycle Oscillation Computations for the NASA Benchmark Supercritical Wing Configuration

Jeffrey P. Thomas and Earl H. Dowell

Duke University, Durham, NC 27708-0300

June 12, 2025

Background and Motivation

- Transonic flutter experiments on a supercritical wing show more complex behavior than at lower Mach numbers.
- The flutter q can dramatically drop as the Mach changes from .7 to .8 and beyond.
- A greater sensitivity to the nominal angle of attack (in both experiments and computations) occurs at the higher Mach number.
- Computations suggest greater sensitivity to structural damping and the viscous boundary layer at the higher transonic Mach numbers.
- Fundamentally, this appears to be associated with (1) a change in flutter mode from coupled mode flutter to single degree of freedom flutter due to negative aerodynamic damping and (2) possibly a flow instability due to shock wave boundary layer interaction (buffet).
- Different CFD models with different grids and different turbulence models can give widely different results.

NASA BSCW Experimental Aeroelastic Configuration

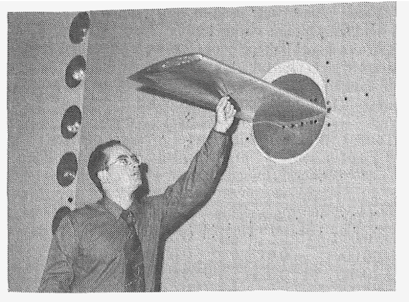

Figure: From Dansberry et al. (1993). AIAA Paper 93-1592.

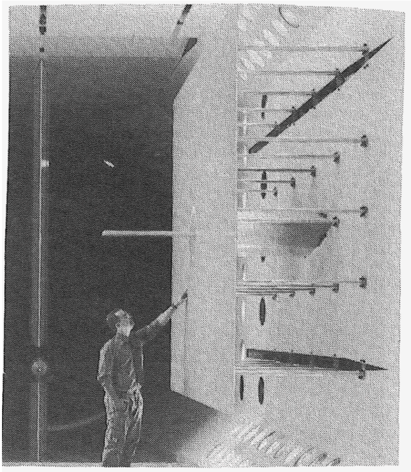

Figure: From Dansberry et al. (1993). AIAA Paper 93-1592.

NASA BSCW Experimental Flutter Onset Results

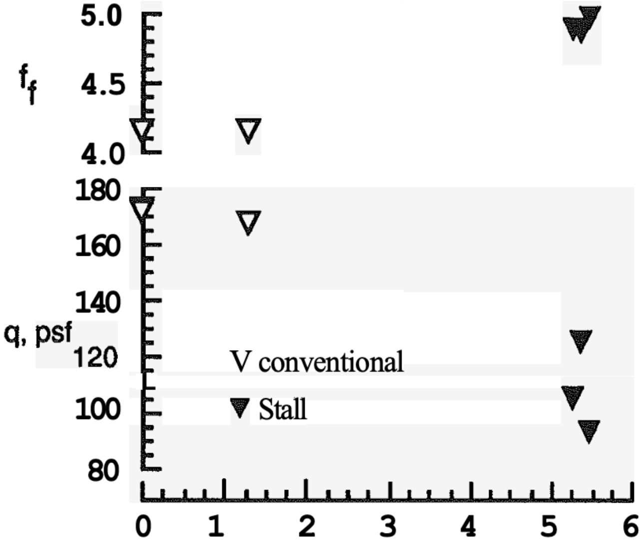

Figure: Frequency and Dynamic Pressure vs. Angle of Attack in Degrees. From Dansberry et al. (1993). AIAA Paper 93-1592.

Objectives and Approach

- Objective #1: Can a two-dimensional computational model predict results in the vicinity of the three-dimensional experimental results for the NASA Benchmark Super-critical Wing (BSCW) configuration?
- Objective #2: What sort of predicted aeroelastic Limit Cycle Oscillation (LCO) trends will the two-dimensional computational model yield? i.e., sub-critical or super-critical LCO response?
- Objective #3: Does the two-dimensional computational model predict transonic flow buffet?

- Approach: A nonlinear frequency domain Harmonic Balance (HB) based Computational Fluid Dynamic (CFD) and aeroelastic solver, which allows for the direct computation of aeroelastic LCO response curves.

Two-Degree of Freedom Airfoil Model

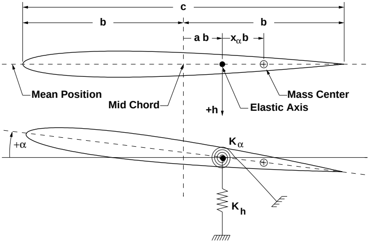

Governing Equations

$$\mathbf{R}(\mathbf{L}, \mathbf{Q}, \chi) = \mathbf{0}$$

$$\mathbf{L} = \begin{Bmatrix} L_1 \\ L_2 \\ L_3 \\ L_4 \\ L_5 \end{Bmatrix} = \begin{Bmatrix} \bar{\alpha}_0 \\ V \\ \bar{\omega} \\ \mathrm{Re}\left(\dfrac{\bar{h}_1}{\bar{\alpha}_1 b}\right) \\ \mathrm{Im}\left(\dfrac{\bar{h}_1}{\bar{\alpha}_1 b}\right) \end{Bmatrix}, \qquad \mathbf{R} = \begin{Bmatrix} R_1 \\ R_2 \\ R_3 \\ R_4 \\ R_5 \end{Bmatrix}$$

$$R_1 = \bar{\alpha}_0 - \alpha_{e_0} - \frac{2V^2}{\pi r_\alpha^2} \bar{c}_{m_0}$$

$$R_2 = \left\{ \frac{\mathrm{Re}(\bar{c}_{l_1})}{\pi \bar{\alpha}_1} - \frac{1}{4} \mu \bar{\omega}^2 \left[\frac{m_h}{m} \mathrm{Re}\left(\frac{\bar{h}_1}{\bar{\alpha}_1 b}\right) + x_\alpha \right] \right\} V^2$$
$$- \sqrt{\mu}\bar{\omega}\zeta_h \left(\frac{\omega_h}{\omega_\alpha}\right) \mathrm{Im}\left(\frac{\bar{h}_1}{\bar{\alpha}_1 b}\right) V + \left(\frac{\omega_h}{\omega_\alpha}\right)^2 \mathrm{Re}\left(\frac{\bar{h}_1}{\bar{\alpha}_1 b}\right)$$

$$R_3 = -\left\{ 2\frac{\mathrm{Re}(\bar{c}_{m_1})}{\pi \bar{\alpha}_1} + \frac{1}{4} \mu \bar{\omega}^2 \left[x_\alpha \mathrm{Re}\left(\frac{\bar{h}_1}{\bar{\alpha}_1 b}\right) + r_\alpha^2 \right] \right\} V^2$$
$$+ r_\alpha^2$$

$$R_4 = \left[\frac{\mathrm{Im}(\bar{c}_{l_1})}{\pi \bar{\alpha}_1} - \frac{1}{4} \mu \bar{\omega}^2 \frac{m_h}{m} \mathrm{Im}\left(\frac{\bar{h}_1}{\bar{\alpha}_1 b}\right) \right] V^2$$
$$- \sqrt{\mu}\bar{\omega}\zeta_h \left(\frac{\omega_h}{\omega_\alpha}\right) \mathrm{Re}\left(\frac{\bar{h}_1}{\bar{\alpha}_1 b}\right) V + \left(\frac{\omega_h}{\omega_\alpha}\right)^2 \mathrm{Im}\left(\frac{\bar{h}_1}{\bar{\alpha}_1 b}\right)$$

$$R_5 = -\left[2\frac{\mathrm{Im}(\bar{c}_{m_1})}{\pi \bar{\alpha}_1} + \frac{1}{4} \mu \bar{\omega}^2 x_\alpha \mathrm{Im}\left(\frac{\bar{h}_1}{\bar{\alpha}_1 b}\right) \right] V^2$$
$$+ \sqrt{\mu}\bar{\omega} V \zeta_\alpha r_\alpha^2$$

Structural Parameters:
$x_\alpha = 0.0$, $r_\alpha^2 = 1.024$, $(\omega_h/\omega_\alpha) = 0.646$,
$\zeta_h = 0.0$, $\zeta_\alpha = 0.0$,
$a = 0.0$

Computational Grid - 193 $\times$ 49 "O-Mesh":

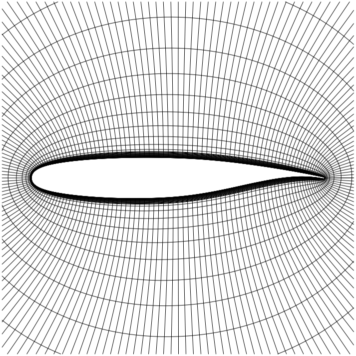

Figure: Computational Grid.

Flow Near the Flutter-Onset Condition, $M_\infty = 0.80$, $Re_\infty \approx 4,000,000$.

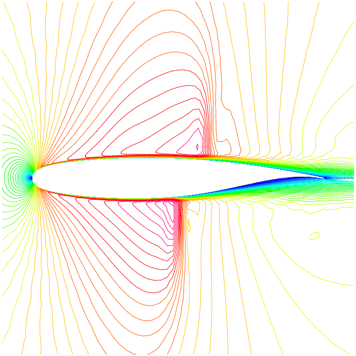

Figure: Mean Flow Mach Number Contours, α_{e_0}=0.0 Degrees.

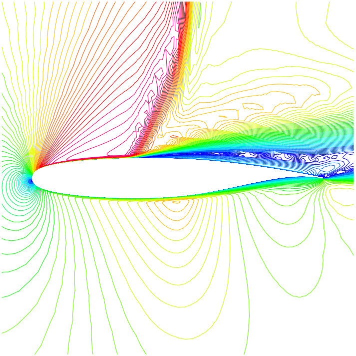

Figure: Mean Flow Mach Number Contours, α_{e_0}=5.0 Degrees.

NASA BSCW Aeroelastic Configuration CFD Grids

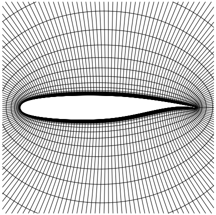

(a) Grid #1 193x49.

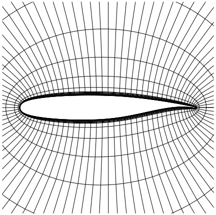

(b) Grid #2 97x25.

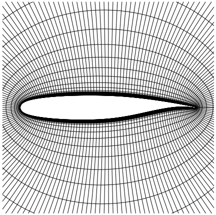

(c) Grid #2 193x49.

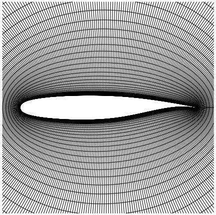

(d) Grid #2 385x97.

NASA BSCW Aeroelastic Configuration Mach Contours at Flutter Onset for $\alpha_{e_0} = 0^{\circ}$ and $\mu = 1000$.

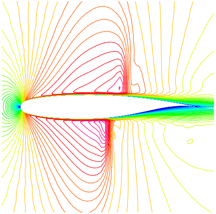

(a) Grid #1 193x49.

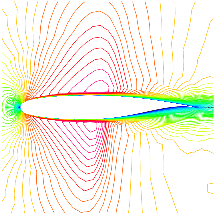

(b) Grid #2 97x25.

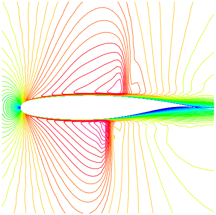

(c) Grid #2 193x49.

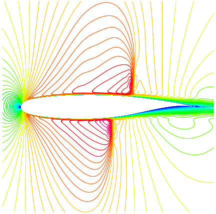

(d) Grid #2 385x97.

NASA BSCW Aeroelastic Configuration Computed LCO Unsteady Pitch Response Trend

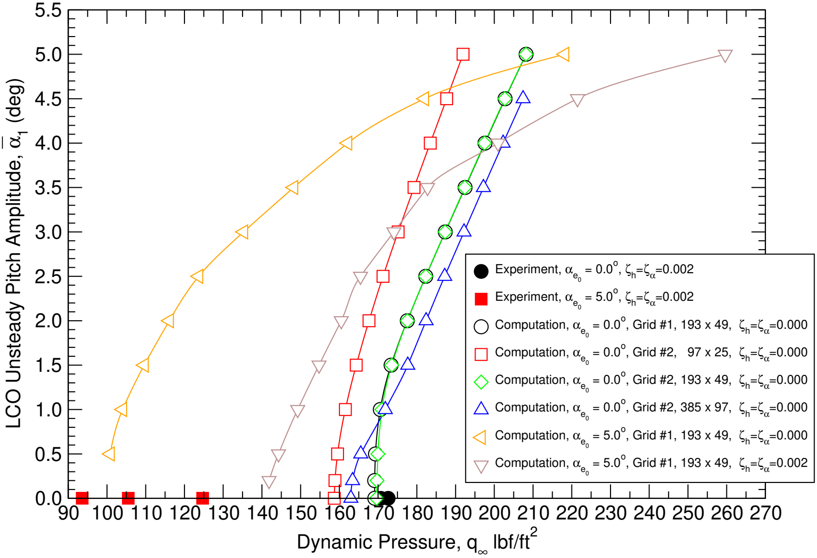

NASA BSCW Aeroelastic Configuration Computed LCO Frequency Response Trend

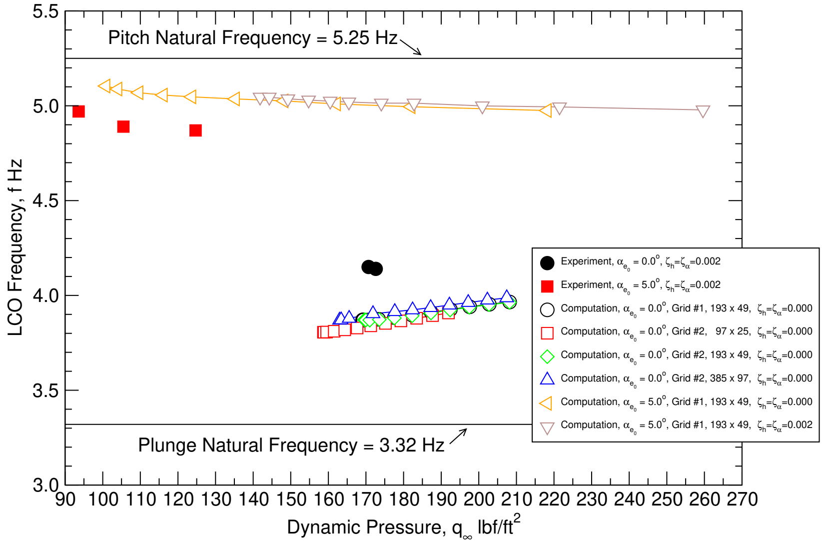

NASA BSCW Configuration Computed LCO Aeroelastic Mode Shape Response Trend

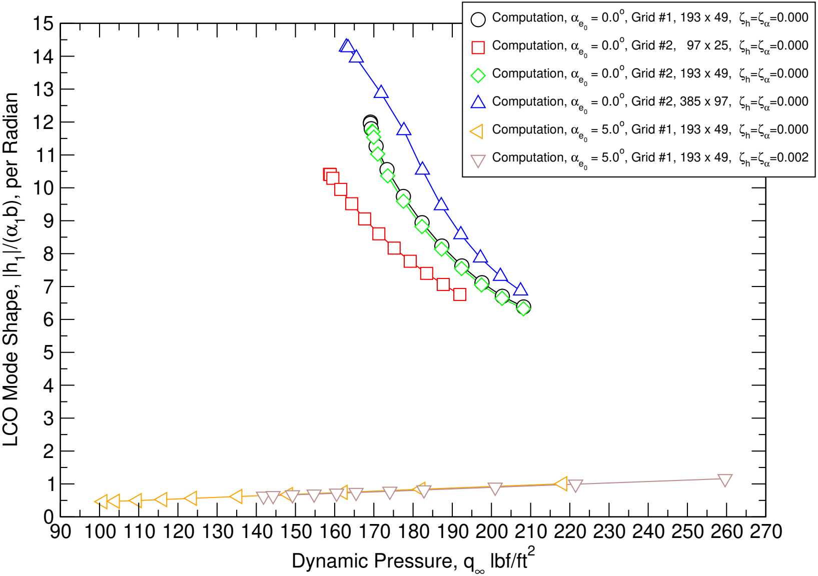

NASA BSCW Aeroelastic Configuration Computed Mean Angle of Attack Response Trend

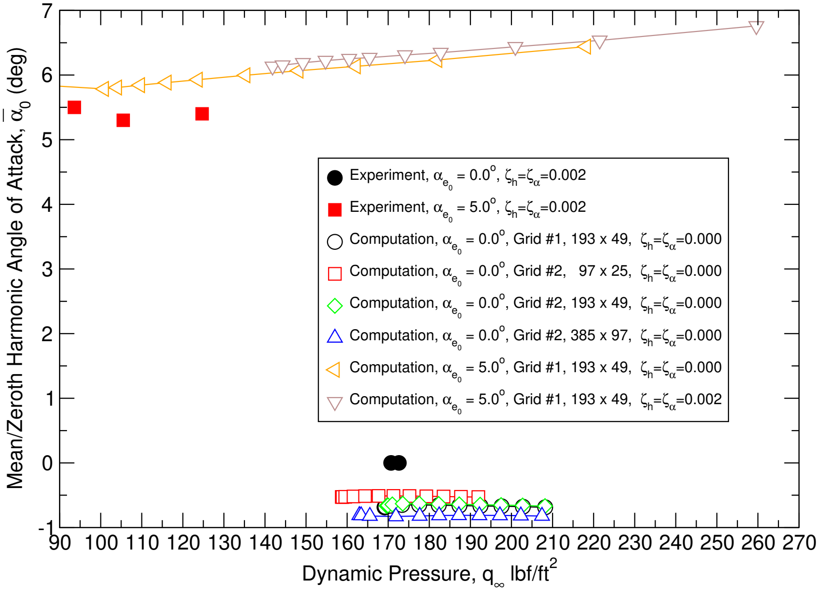

NASA BSCW Aeroelastic Configuration Computed LCO Unsteady Pitch Response Trend

Note: Reynolds Number is Fixed at $Re = 4006103$ for Computations.

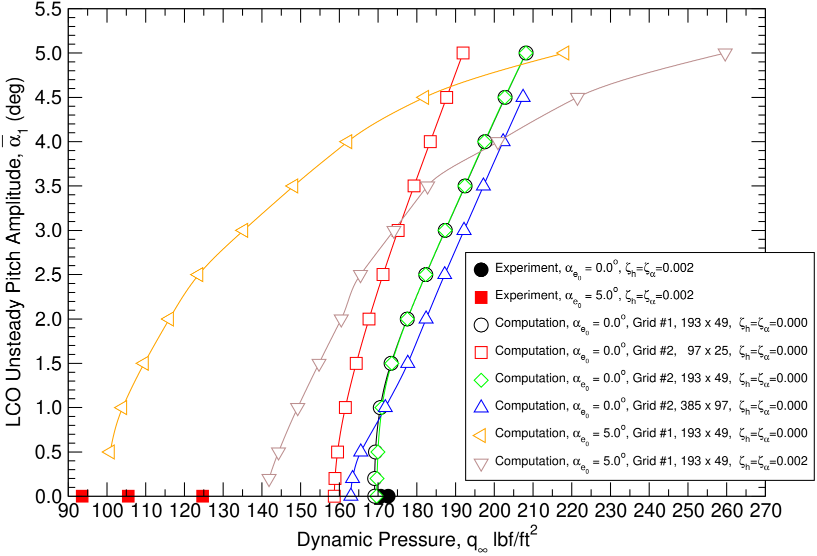

NASA BSCW Aeroelastic Configuration Experimental Flutter Results

Table 6. Experimental results in R-12 with fixed transition using #35 grit.

Tab Point no.	α_m deg	M	q lb/ft^2	a ft/sec	V ft/sec	ρ slugs/ft^3	R_n x10^{-6}	μ	V_I	f_f Hz	f_f/f_2	k	Z Mag in.	Z Phase deg	θ Mag deg
492	-0.3	.44	157.4	506.5	220.4	.006482	5.268	253	.72	4.53	.87	.0861	.28	-172.5	1.20
488	-0.2	.58	162.4	508.0	294.2	.003752	4.075	437	.75	4.45	.86	.0633	.29	-174.0	1.03
485	-0.2	.69	169.3	507.9	350.0	,002764	3.579	593	.79	4.35	.84	.0521	.49	-174.7	1.42
480	-0.1	.74	168.8	5M.6	375.7	.002392	3.340	685	.79	4.30	.83	.0480	.38	-175.2	1.01
465	0.0	.80	172.6	510.9	407.4	.002080	3.113	788	.84	4.14	.80	.0425	.70	-173.9	1.40
472	0.0	.80	170.7	510.0	409.3	.002038	3.072	805	.83	4.15	.80	.0424	.37	-174.8	0.73
457	1.3	.80	166.9	509.7	407.3	.002012	3.022	815	.82	4.14	.80	.0425	.35	-174.5	0.69
470	0.0	.82	178.8	511.5	417.7	.002050	3.141	800	.87	4.05	.78	.0407	.62	-173.4	1.01
466	0.0	.82	177.5	510.0	419.7	.002016	3.116	813	.85	4.13	.79	.0412	.24	-174.5	0.42
427	5.4	.80	1'24.7	507.2	406.1	.001512	2.281	1084	.60	4.87	.94	.0503	.08	-162.9	0.69
403	5.3	.80	105.5	505.6	404.0	.001293	1.951	1268	.55	4.89	.94	.0507	.05	-168.0	0.43
395	5.5	.80	93.6	503.6	402.0	.001158	1.749	1416	.51	4.97	.96	.0518	.08	-167.5	0.90

NASA BSCW Aeroelastic Configuration Computed LCO Unsteady Pitch Response Trend

Note: Reynolds Number is Fixed at $Re = 4006103$ for Computations.

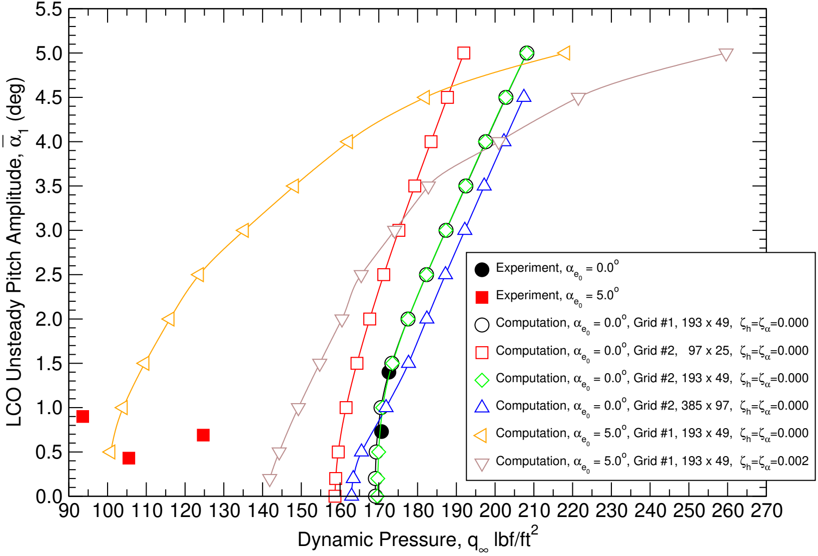

NASA BSCW Configuration Computed LCO Aeroelastic Mode Shape Response Trend

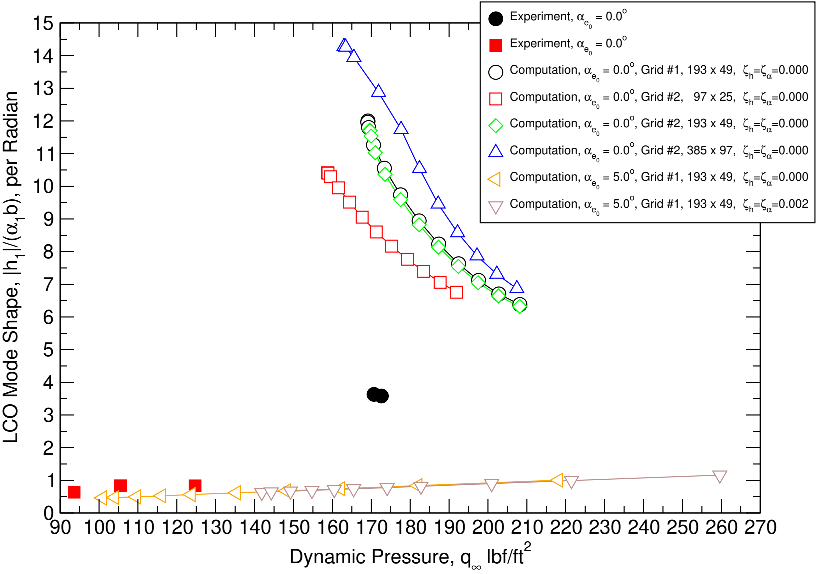

NASA BSCW Aeroelastic Configuration Wind Tunnel Flow Conditions

Parameter	Units													
Mach		0.799	0.8	0.8	0.8	0.8	0.8	0.8	0.8	0.8	0.8	0.8	0.801	0.801
qbar	psf	10.02	25	35	50	75	100	134	143	152	168.8	200	225	250
Mach	1/ft	0.799	0.8	0.8	0.8	0.8	0.8	0.8	0.8	0.8	**0.8**	0.8	0.801	0.801
qbar	psf	10.02	25	35	50	75	100	134	143	152	**168.8**	200	225	250
Rec		237461	592224	829213	1184801	1777732	2371336	3178880	3392751	3606668	**4006103**	4748658	5343835	5939368
Re	1/ft	178096	444168	621910	888601	1333299	1778502	2384160	2544563	2705001	**3004577**	3561493	4007876	4454526
V	ft/s	440.45	440.63	440.59	440.51	440.39	440.21	440.05	440	439.96	**439.88**	439.7	439.58	439.46
a	ft/s	551.08	550.94	550.85	550.71	550.48	550.25	549.94	549.86	549.78	**549.62**	549.34	549.11	548.88
T_static	deg_F	80.87	80.83	80.83	80.82	80.81	80.8	80.78	80.77	80.77	**80.76**	80.74	80.73	80.71
rho	slugs/ft3	0.000103	2.58E-04	0.000361	0.000515	0.000774	0.001032	0.001384	0.001477	0.001571	**0.001745**	0.002069	0.002329	0.002589
gamma		1.1121	1.1122	1.1123	1.1124	1.1126	1.1128	1.1131	1.1131	1.1132	**1.1133**	1.1136	1.11E+00	1.1139
mu	lb-sec/ft2	2.56E-07	2.56E-07	2.56E-07	2.56E-07	2.56E-07	2.56E-07	2.55E-07	2.55E-07	2.55E-07	**2.55E-07**	2.55E-07	2.55E-07	2.55E-07
Pr		0.68394	0.68404	0.6841	0.68419	0.68435	0.6845	0.68471	0.68477	0.68483	**0.68493**	0.68513	0.68528	0.68544
H	psf	40	99.7192	139.609	199.446	299.181	399.003	534.692	570.612	606.532	**673.587**	798.205	898.014	997.829
P	psf	28.2069	70.3193	98.4486	140.644	210.975	281.366	377.05	402.38	427.711	**474.996**	562.873	633.255	703.643
T_stagnation		100	100	100	100	100	100	100	100	100	**100**	100	100	100
X		0.95	0.95	0.95	0.95	0.95	0.95	0.95	0.95	0.95	**0.95**	0.95	0.95	0.95

NASA BSCW Aeroelastic Configuration Computed LCO Unsteady Pitch Response Trend

Effect of Matching Reynolds Number in Computations.

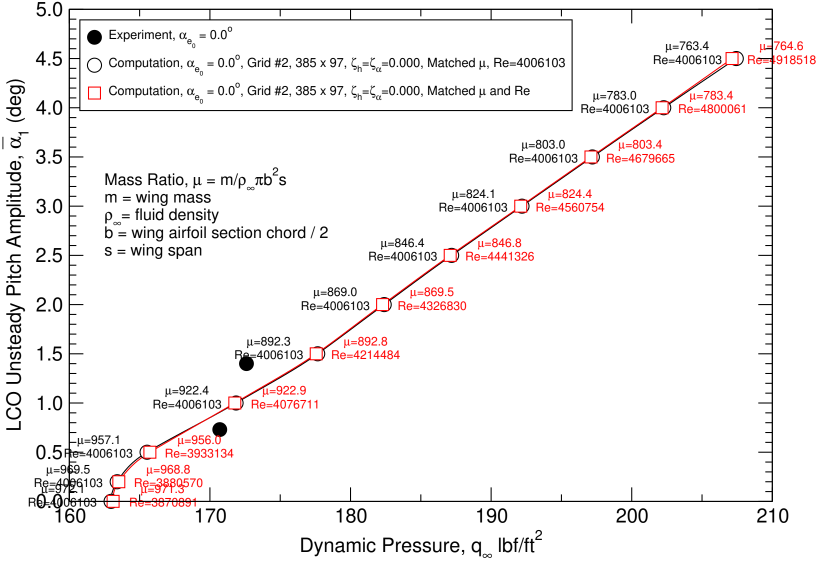

NASA BSCW Aeroelastic Configuration Computed LCO Unsteady Pitch Response Trend

Effect of Matching Reynolds Number in Computations.

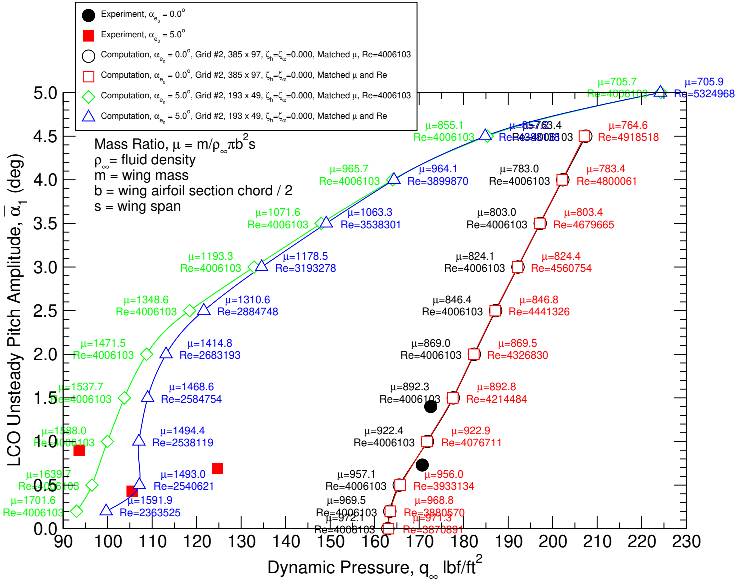

NASA BSCW Aeroelastic Configuration Computed LCO Unsteady Pitch Response Trend

Harmonic Convergence.

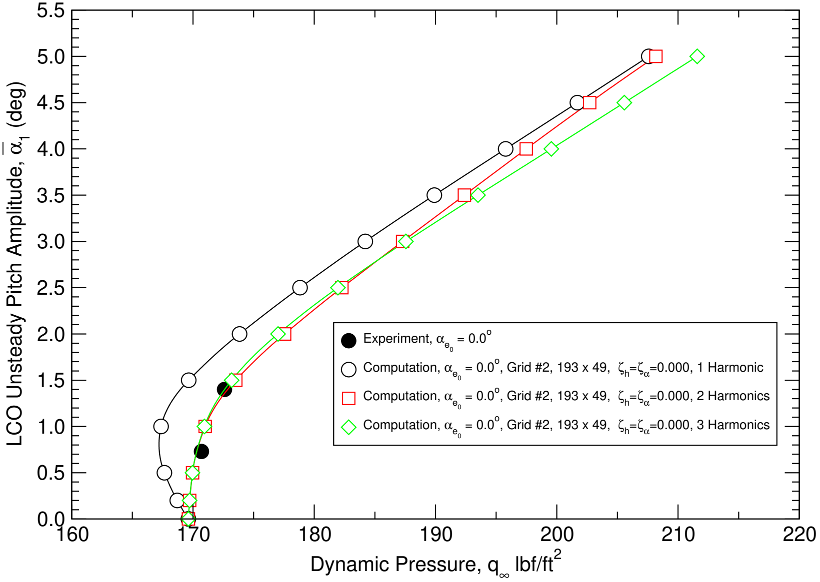

NASA BSCW Aeroelastic Configuration Computed LCO Unsteady Pitch Response Trend

Structural Damping Effect.

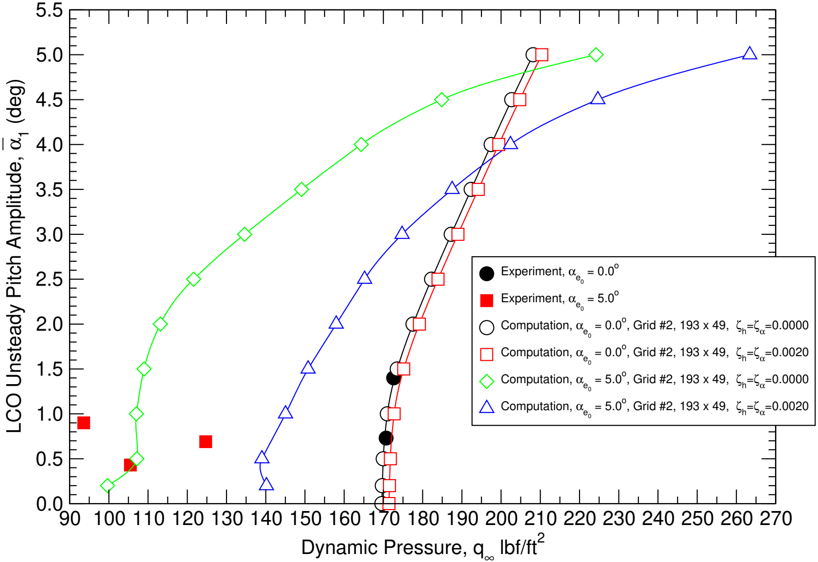

NASA BSCW Experimental Aeroelastic Configuration Measured Structural Damping

NASA Technical Memorandum 4457

Physical Properties of the Benchmark Models Program Supercritical Wing

Bryan E. Dansberry, Michael H. Durham,
and Robert M. Bennett
Langley Research Center
Hampton, Virginia

David L. Turnock
Lockheed Engineering & Sciences Company
Hampton, Virginia

Walter A. Silva and José A. Rivera, Jr.
Langley Research Center
Hampton, Virginia

NASA
National Aeronautics and
Space Administration
Office of Management
Scientific and Technical
Information Program
1993

Figure: Dansberry et al. (1993). NASA TM 4457.

NASA BSCW Experimental Aeroelastic Configuration Measured Structural Damping

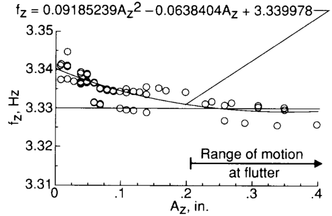

Figure 17. Wind-off frequency for plunge mode.

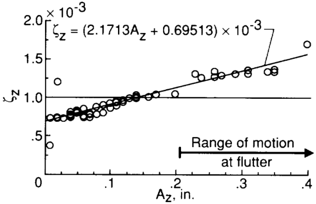

Figure 19. Wind-off damping for plunge mode.

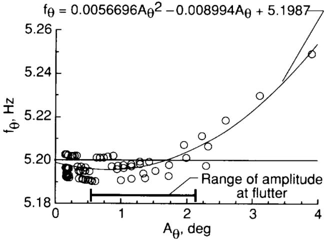

Figure 18. Wind-off frequency for pitch mode.

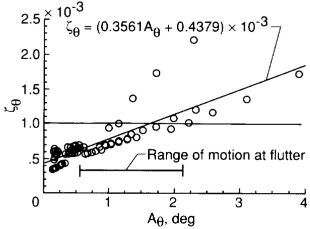

Figure 20. Wind-off damping for pitch mode.

Figure: From Dansberry et al. (1993). NASA TM 4457.

NASA BSCW Aeroelastic Configuration Computed LCO Unsteady Pitch Response Trend

Effect of Variable Structural Damping.